This is a non-peer reviewed preprint submitted to EarthArXiv. This manuscript has been accepted for review in *Geostandards and Geoanalytical Research*. Please note that this manuscript has yet to undergo peer review and subsequent versions may have slightly different content.

The Heavy Mineral Map of Australia Project: A Novel, Rapid, Automated Quantitative Mineralogy Workflow

Journal:	*Geostandards and Geoanalytical Research*
Manuscript ID	Draft
Manuscript Type:	Original Article
Date Submitted by the Author:	n/a
Complete List of Authors:	Walker, Alexander; Curtin University, John de Laeter Centre McInnes, Brent; Curtin University, John de Laeter Centre de Caritat, Patrice; Geoscience Australia Bastrakov, Evgeniy; Geoscience Australia
Keywords:	mineral exploration, heavy minerals, mineral network analysis, automated mineralogy, mineralogy

SCHOLARONE™
Manuscripts

The Heavy Mineral Map of Australia Project: A Novel, Rapid, Automated Quantitative Mineralogy Workflow

Alexander T. Walker[a], Brent I. A. McInnes[a], Patrice de Caritat[b], Evgeniy Bastrakov[b]

[a]*John de Laeter Centre, Curtin University, WA, Australia*

[b]*Geoscience Australia, Canberra, ACT, Australia*

Alexander Walker: a.walker@curtin.edu.au

Brent McInnes: directorjdlc@curtin.edu.au

Patrice de Caritat: patrice.decaritat@ga.gov.au

Evgeniy Bastrakov: evgeniy.bastrakov@ga.gov.au

For Review Only

Abstract

The Heavy Mineral Map of Australia (HMMA) is the world's first project aiming to define a continental heavy mineral baseline. It utilises a novel sample processing workflow and automated mineralogy techniques to rapidly generate and analyse mineralogical data from 1315 archived samples of catchment outlet sediments collected from 1186 catchments across the Australian continent.

Heavy minerals were extracted and concentrated from the 75–425 µm fraction of each sample via an optimised workflow to accelerate output while maintaining integrity and quality of produced heavy mineral concentrates. Automated mineralogy facilitated rapid and consistent collection of mineral data from each heavy mineral concentrate, and an associated bespoke mineral library incorporates more than 160 unique mineral phases, including minerals that will be of interest to both researchers and mineral explorers. A publicly accessible mineral network analysis application has been developed in parallel with the HMMA project to facilitate exploration and interpretation of the resulting >140 million mineral grain identifications dataset.

Upon completion in late 2023 the HMMA will provide a heavy mineral baseline across approximately 80% of Australia, with processing of samples and data acquisition undertaken in a standardised and uniform manner enabling easy replication of techniques and both internal and external comparability.

Keywords: heavy minerals, mineralogy, automated mineralogy, mineral exploration, mineral network analysis

For Review Only

1. Introduction

The Heavy Mineral Map of Australia (HMMA) project is a collaboration between Geoscience Australia (GA) and Curtin University that aims to define a heavy mineral (HM) baseline across Australia (Caritat *et al.* 2022). It utilises HM concentrates extracted from samples of catchment outlet sediments previously collected as part of the National Geochemical Survey of Australia (NGSA), to date Australia's only consistent continental-scale geochemical dataset and atlas (Caritat 2022). HMs are defined here as minerals with a specific gravity greater than 2.9 g/cm^3. The HM fraction of the catchment outlet sediments contains several useful minerals including zircon, apatite and rutile, which have utility for geochronology and petrochronology, in addition to a wide range of so-called indicator minerals; those minerals whose presence may indicate the occurrence of geological processes associated with specific mineral deposits, alteration or rock lithology (McClenaghan 2005).

An optimised workflow was developed to process the 1315 HMMA samples for heavy mineral content at facilities within the John de Laeter Centre at Curtin University. Automating the mineralogical analysis of the resulting heavy mineral concentrates (HMCs) was essential to ensure delivery of mineral data on a reasonable timescale; a single mounted sample of HMC containing thousands or tens of thousands of mineral grains can be analysed by automated mineralogical techniques within an hour, versus the tens or hundreds of grain analyses that can be undertaken per hour via manual SEM analysis. Further, the resulting continental scale dataset is large and multidimensional; more than 140 million mineral observations classified into more than 160 unique mineral phases across 1315 samples. Consequently, novel data analytics and visualisation techniques needed to be developed in parallel with the data acquisition workflow to facilitate data exploration and interpretation.

For Review Only

2. Sample materials

The HMMA provides heavy mineral data for NGSA project samples collected using the sampling methodology of Lech *et al.* (2007). A brief overview of the sampling rationale is presented here.

A total of 1315 samples (including field duplicates) were collected from 1186 catchments across Australia with a sampling density of approximately 1 sample per 5200 km^2. Sampled material consists of catchment outlet sediments (similar to overbank or floodplain sediments). Catchment outlet sediments are deposited outside riverbanks as floodwaters recede and may be modified by aeolian processes following deposition (Caritat 2022). Two samples were taken from each site, one at 0–10 cm depth, the other on average between 60–80 cm below the surface, referred to as Top Outlet Sediment (TOS) and Bottom Outlet Sediment (BOS), respectively. These sediments are reasonably assumed to represent well mixed, fine-grained composites of major soil and rock types present in the upstream catchment(s) (Caritat 2022). The HMMA utilises BOS sample materials as these are most likely to comprise geologic material unaffected by post-depositional anthropogenic inputs (e.g. fertilisers). Further, by selecting a 75–425 µm grain size fraction for HM extraction in order to avoid mineral input due to aeolian processes.

NGSA sampled sites are identified with the prefix 200719 followed by a four-digit unique identifier (SampleID) between 0001 and 1600. SampleIDs were assigned randomly and thus carry no spatial information or inference, and field duplicates have SampleIDs independent of the original samples (thus not identifiable as duplicates without a lookup file). Field duplicates were collected at ~10 % of the NGSA sites, at a median distance of ~100 m from the original site.

For Review Only

3. Methods

3.1 Sample Preparation

Following drying and homogenisation in the laboratory at GA, the TOS and BOS samples were first split approximately 50:50 into an analytical sample and an archive sample, the latter being stored at GA for future investigations. The analytical sample was separated into 'bulk', 'coarse' (<2 mm), and 'fine' (<75 µm) fractions. The latter two fractions were subjected to the comprehensive geochemical analysis programme of the NGSA, which included up to three different geochemical digestions and determination of the concentrations of about 60 elements (Caritat, 2022). The bulk samples were reserved for mineralogical analysis, including spectral mineralogy (Lau et al., 2016), X-ray diffraction analysis (Caritat & Troitsch 2021, Caritat *et al.* 2023), and this heavy mineral assay project. The 1315 bulk NGSA BOS samples were sent to the John de Laeter Centre at Curtin University for processing and analysis for the HMMA project. Samples were processed for heavy mineral content according to the workflow illustrated in Figure 1.

[Approximate position of Fig. 1 here]

Bulk samples (labelled A in Figure 1) are weighed on arrival (step 1) and then dry sieved (2) through stacked 2000 µm, 430 µm and 75 µm sieves on a shaker table to produce >2 mm (B), <2 mm to >430 µm (C), <430 µm to >75 µm (D) and <75 µm (E) fractions. Fractions B, C, and E are weighed and archived (3, 4, 5, 7). Fraction D is weighed and riffle split into fractions D1 and D2 using a 3-D printed riffle splitter (Fig. 2) (6), D1 is weighed and archived, and D2 is weighed and retained for further processing.

At this point in traditional heavy mineral separation workflows, samples would be mixed with a 'heavy' liquid such as sodium polytungstate, decanted into funnels, allowed to slowly

For Review Only

separate, and then gradually siphoned off to recycle the heavy liquids and remove the now separated 'heavy' and 'light' mineral fractions (e.g. Callahan 1987). This process is time-consuming and requires large volumes of expensive heavy liquids; this is impractical given the number of samples used for the HMMA. Instead, a cryogenic workflow comparable to Morrow & Webster (1989) is used. D2 fractions were mixed with lithium-heteropolytungstate (LST), decanted into vials and centrifuged at 1500 rpm for 15 minutes (9) to separate the heavy and light mineral fractions. The tip of each vial is then submerged within liquid N_2 to freeze the HMC, and to allow immediate and easy decanting of the LST and its contained light mineral concentrate (LMC) (10). The LMC is filtered, rinsed, dried, weighed, and archived (F), and the LST recycled (11). The frozen HMC/LST mixture is thawed, the HMC is filtered, rinsed, weighed, and the LST recycled (12, 13, 14). The HMC is retained for further processing.

[Approximate position of Fig. 2 here]

[Approximate position of Fig. 3 here]

If the mass of HMC for a sample is greater than approximately 0.5 g, it is riffle split into HMC1 and HMC2, where HMC1 is weighed and archived (15) and HMC2 is weighed and proceeds to mounting. Each HMC2 is embedded within a 25 mm cylindrical epoxy mount alongside a 3D-printed three-sided plastic template. Where the mass of HMC of a sample still exceeds that needed for mounting, the 'cone and quarter' method is used to generate a representative subsample (e.g. Udayakumar et al., 2020). The template provides a spatial reference feature on the upper sample surface while also supporting a label on the back of the mount with sample identity details and a scannable QR code (Fig. 3). Scanning the latter with a smartphone or tablet brings up a sample metadata URL including a sample location map. The upper surface of the mount containing mineral grains is then polished to a 1 µm finish, cleaned, dried, and carbon coated for analysis (17).

For Review Only

3.2 Automated mineralogy

3.2.1 Overview of TIMA functionality

The configuration of the TESCAN Integrated Mineral Analyser (TIMA) operating at the John de Laeter Centre at Curtin University comprises four fully integrated silicon drift Energy Dispersive Spectroscopy (EDS) X-ray detectors linked to a TESCAN MIRA field emission gun (FEG) platform. It is optimised to provide high data throughput, by using multiple EDS detectors to rapidly acquire elemental spectra which are subsequently used to identify mineralogy at each measurement point. The TIMA may be operated in one of four modes: point spectrometry, line mapping, high resolution mapping and dot mapping (Fig. 4).

In *point spectrometry mode*, the identification of particles and grains is determined solely by back-scattered electron (BSE) images; areas of equivalent BSE brightness are defined as discrete regions, and the centre of the largest inscribed circle of each region is used as the location of an EDS analysis point to identify a mineral for each given region (Hrstka *et al.* 2018). Point spectrometry enables rapid analysis of samples but with a significant risk of misclassification, as it will not discriminate between two adjacent areas with similar BSE brightness but different chemistry (e.g., pyroxenes, amphiboles).

In *line mapping mode* a sample surface is analysed along equidistant lines using a specified line spacing and a specified pixel spacing for BSE/EDS measurements. Following scan completion the lines are subdivided into sections with a combination of the collected BSE and EDS data used to determine mineral boundaries (Hrstka *et al.* 2018). Line mapping is relatively rapid and can differentiate between minerals of similar BSE brightness, but provides ‘slices’ through analysed material rather than comprehensive quantitative textural information.

[Approximate position of Fig. 4 here]

For Review Only

In *high resolution mapping mode* the TIMA collects BSE measurements over a specified spacing with an EDS measurement also taken at each BSE point. High resolution mapping is the most time-intensive scanning mode, taking approximately 30 minutes to analyse a 1 cm^2 area of rock using 10 µm pixel spacing and 1000 counts per EDS spectrum (Hrstka *et al.* 2018), but provides the highest resolution textural data.

In *dot mapping mode* BSE measurements are taken in a grid over the sample with a specified pixel spacing; areas of equivalent BSE brightness are combined into discrete segments and greatest inscribed circles are used to find centre points for each segment. A grid of EDS measurements with specified spacing is taken over each of the segments, with the combined BSE and EDS data then used to refine the segmentation and differentiate between minerals of similar BSE brightness but different chemistry; where multiple EDS measurements are taken within a chemically homogenous segment, the EDS signals are summed to produce a single higher quality spectra per refined segment (Hrstka *et al.* 2018). The HMMA project utilises dot mapping as this mode provides an excellent trade-off between analytical time and data quality.

Mineral assays reported for sample mounts in this study were acquired via the TIMA operated at 25 kV with a probe current of 5.31 nÅ and a spot size of approximately 89 nm. Samples were analysed in dot mapping mode with a BSE measurement step distance of 3 µm and an EDS spot step distance of 27 µm. Sample analysis was conducted over a period of approximately 18 months, with TIMA EDS performance monitored using an ASTIMEX international standard mount containing 50 minerals of known chemical composition (MINM25-53 +FC Serial 1AQ; Astimex Standards Limited (https://www.astimex.com).

For Review Only

3.2.2 TIMA mineral classification

Following SEM-EDS analysis of the surface of the heavy mineral mount, the x-ray spectra for each grain are compared to a linked library of mineral phases comprising real and simulated spectra generated from the online Webmineral database (https://www.webmineral.com). Mineral names and associated properties are assigned to grains where a mineral match is found. Element peak intensity rules that characterise each mineral definition are designed by the user and utilise element peak intensity thresholds, which may be populated either by the user or automatically populated by the TIMA software based on spectra associated with the specific mineral definition (Fig. 5). The operator should exercise caution when expanding the library to prevent clashes and misclassification issues, particularly when adding new minerals with similar compositions to existing entries, which may necessitate additional element rules for accurate discrimination. Once mineral classification is considered satisfactory for a sample, a panoramic view of sample mineralogy can be generated (Fig. 6).

[Approximate position of Fig. 5 here]

[Approximate position of Fig. 6 here]

4. Results and Discussion

The HMMA dataset totals more than 140 million individual mineral grains observations from 1315 samples covering ~81% of Australia. Mineral assay data released for the HMMA project comprise mineral abundances reported as absolute observation counts, relative (per 1000) observation counts, as well as in mass percent, volume percent. Supplementary information on grain size distributions for each mineral are also provided and summarised

For Review Only

using median values. TIMA mineral data are compiled, organised and integrated with sample metadata using a Python script. Sample metadata includes analysis date (year), the latitude/longitude of the location sampled, the associated Geoscience Australia EFTF deep-dive area (where applicable), and a 'Yield' value which is a unitless number indicating the relative HM abundance between samples, derived by dividing the HM mass by the D2 mass for each sample (see Sample Preparation and Fig. 1). Partial HMMA datasets for the Darling-Curnamona-Delamerian (DCD) and the Barkly-Isa-Georgetown (BIG) test regions have been released (Caritat *et al.* 2022a, 2022b).

The TIMA mineral library associated with the HMMA project includes approximately 160 phases (Appendix A). More than 90% of these phases are unique IMA-recognised minerals, however several entries diverge from the IMA vocabulary. This is typically due to factors such as the presence of mineral solid solutions or minerals with identical chemical compositions (the aluminosilicate polymorphs kyanite, andalusite and sillimanite, for example). Several minerals may also not be reliably identified or differentiated between via TIMA due to overlapping EDS spectra, an issue especially prominent when attempting to identify specific amphibole, mica or pyroxene species. Appendix A documents all mineral entries within the HMMA mineral library and identifies where there may be difficulties with identification or misclassification.

For Review Only

4.1 Testing for contamination

4.1.1 Fe-Cr alloy content within samples

Grains of what appears to be an iron-chromium alloy were noted in approximately 960 samples with abundances of 1–316 grains, with a median abundance of 2 grains. (Fig. 7). These grains are identified mineralogically as chromferide (Fe_3Cr_{1-x} (x=0.6)), the occurrence of which has been documented in impact melt rocks (e.g. Gurov *et al.* 2019) and as an accessory mineral in ore deposits (Novgorodova *et al.* 1986), but may also be

compositionally consistent with stainless steel; a common material in laboratory fittings and equipment, but most notably in some of the sieves used within the HMMA sample preparation methodology.

New, clean polishing discs were used to polish HMMA samples, ruling out contamination of mounted samples by shared polishing materials used for materials science projects in the John de Laeter Centre. To determine whether contamination during sieving was responsible for the observed chromferide grains, testing of sieving procedures was undertaken using nearly pure silica sand (containing ~0.01–0.02 % Fe). Four aliquots of silica sand were taken for testing, with one aliquot concentrated and mounted without sieving as a control sample, and the remaining three aliquots were passed through stainless steel sieve stacks for one, two, or three sieving cycles, and subsequently concentrated and mounted. All mounted silica sand samples were analysed by TIMA using the same analytical parameters and mineral library associated with HMMA samples.

[Approximate position of Fig. 7 here]

Mineralogical analysis indicates the presence of 2–3 grains of chromferide (<10 μm) in all of the silica sand HMCs including the control sample (Fig. 8). Given the presence of chromferide within the unsieved control sample we conclude that use of stainless-steel sieves does not contaminate sieved material, and the chromferide observed in the silica sand is in fact ‘background’ derived from whatever processes have been used to purify the sand. Further, these chromferide grains are significantly smaller than those observed in HMMA samples, and therefore we conclude that chromferide in the HMMA 75–425 μm data are of natural origin.

For Review Only

4.1.2 Cu-Zn alloys

One hundred and seventy-eight HMMA samples contain 1–34 grains of a zinc-copper alloy identified as tongxinite (Cu_2Zn). Tongxinite is currently unrecognized by the International Mineralogical Association but has been reported in Chinese base metal deposits (e.g. *Xie et al.* 2006); it also has a composition similar to brass, which is present within some sieves used in the sample preparation workflow. A test similar to that conducted for chromferide was used to determine whether tongxinite content in samples is 'real' or contamination; three aliquots of pure silica sand were sieved through brass sieve stacks for one, two, or three sieving cycles, subsequently concentrated, mounted, and polished for TIMA analysis. No brass particles were observed in the mounts of silica sand and, given that brass is not used elsewhere within the HMMA workflow, tongxinite observed within HMMA samples is considered here to be of natural origin.

[Approximate position of Fig. 8 here]

4.2 Quality assessment

4.2.1 Comparison of field duplicate samples

Duplicate samples were taken from 133 sample sites to allow assessment of variations in heavy mineral content across different samples from the same HMMA site. The list of duplicate site IDs may be found in Cooper *et al.* (2011).

[Approximate position of Fig. 9 here]

Abundances of chromite, florencite, gahnite, ilmenite, rutile, and zircon, all commonly reported within the dataset, have been used to demonstrate variability in mineral presence between six original sites and the associated duplicate sites in Table 1. Presence or

For Review Only

absence, rather than observation counts, volume percent or mass percent data, is used to assess consistency between field duplicate pairs (Fig. 9). Where minor/trace minerals such chromite, florencite and gahnite occur in an original sample they typically occur in the duplicate field sample, although significant uncertainty may arise where observations of minerals in question are below approximately 20 counts; chromite is present in 5 of 6 original samples but all 6 of the duplicate field samples, whereas gahnite co-occurs in only 3 original-duplicate sample pairs (Fig. 9). Differences in observation counts for the selected minerals between the original and duplicate field samples are less than 3% when normalised to the total observation population in a sample (Table 1).

4.2.2 Comparison of laboratory duplicate samples

Duplicate mounts were made for six samples with surplus HMC to assess reproducibility through the utilised sample preparation workflow (laboratory duplicates). Abundances of chromite, florencite, gahnite, ilmenite, rutile, and zircon have again been used to assess differences in mineral abundances between original and lab duplicate sample mounts; TIMA-derived mineralogical results for the six original samples and their lab duplicates may be found in Table 2.

Differences in the highlighted mineral abundances as proportions of total mineral counts between samples and duplicates are generally less than 4% (Table 2), apart from 2007191372 where there is an 11.5 % discrepancy in ilmenite abundance.

4.2.3 Comparison of TOS-BOS samples

Prior to the HMMA a pilot project was undertaken by Caritat *et al.* (2022) to test the heavy mineral content in the NGSA sample set. For this pilot project, TOS samples were used. The results of statistical analysis of heavy mineral contents from the 10 sample sites featured in

For Review Only

the pilot project are presented here to compare heavy mineral abundances in TOS and BOS samples from the same sites.

The minerals featured in Table 3 were selected on the basis of having median observations >1 in both the TOS and BOS samples, being relatively common and/or having possible utility as an indicator mineral. Mineral data was Box-Cox transformed to bring them closer to a normal distribution. Correlation coefficients drawn from the transformed weight percent data tend to be the most positive, including the highest coefficient values for 8 of the 12 selected minerals and the highest coefficient values overall (0.96 for staurolite and biotite).

[Approximate position of Table. 1 here]

[Approximate position of Table. 2 here]

[Approximate position of Table. 3 here]

Reasonably strong levels of correlation exist across several minerals identified in TOS and BOS samples overall, indicating consistency of mineralogy in samples taken in the same locations at different depths, and may reduce uncertainty around representative sampling methodologies for heavy mineral surveys similar to the HMMA in future.

4.2.4 Comparison of mineralogy and geochemistry

To determine how mineralogical and geochemical data from the HMMA compare, aliquots of D1 (75–425 μm) material from twelve HMMA samples were sent for whole-rock geochemical analysis. The HMMA material was analysed at Intertek Genalysis using a lithium-borate fusion followed by XRF and LA-ICP-MS analysis (LITH204 method).

For Review Only

An investigation was conducted into correlation between Zr and zircon contents, and rutile/ilmenite and Ti contents. To facilitate easier comparison of Ti and titanium mineral contents, ilmenite mass in each of the samples has been converted to equivalent rutile mass on the basis of its titanium content, and a total rutile content calculated.

[Approximate position of Fig. 10 here]

No positive correlation is observed for HMMA D1 Ti/Zr content and equivalent rutile/zircon mass (Fig. 10); an absence of positive correlation was also observed between NGSA (<2 mm) Ti/Zr content and equivalent/rutile content. Despite the significance of rutile and ilmenite as hosts for titanium, a lack of positive correlation between Ti and rutile/ilmenite content could be explained by the presence of other titanium-bearing minerals such as pseudorutile or pseudobrookite, or by the common substitution of Ti for other elements in many minerals present within HMMA material (e.g., Ti-biotite). More curious is the absence of correlation between Zr and zircon contents, especially given the positive correlation seen between zircon and Zr in the pilot project that preceded the HMMA (Caritat *et al.* 2022a). Zircon ($ZrSiO_4$) is the most significant Zr-bearing mineral in the HMMA dataset, while baddeleyite (ZrO_2) is also present but occurs in trace concentrations (0.001 mass percent on average across all samples). Theoretically, a correlation between Zr and zircon content should exist; additional research is necessary to understand the reasons for the lack of such correlation in these samples. We note, however, that the earlier positive correlation of the pilot project data was based on the NGSA's total acid digestion (including HF) of the lithium-borate flux pellets followed by ICP-MS, which was found by Caritat & Cooper (2011; their figure 9) to faithfully reflect a true total analysis for Zr as independently determined by XRF; the geochemical analysis of the HMMA aliquots used XRF and LA-ICP-MS to determine Ti and Zr contents, respectively.

For Review Only

4.3 Applications for the HMMA heavy mineral dataset

The wide range of minerals classified within HMMA samples is relevant to multiple areas of applied research, such as the utilisation of indicator minerals (e.g., gahnite ($ZnAl_2O_4$), ecandrewsite ([Zn,Fe,Mn]TiO_3), cassiterite (SnO_2) and base metal sulfides) within the HMMA dataset as potential exploration vectors to mineralisation (Fig. 11). In addition, certain essential rock-forming minerals, or minerals of geochronological interest (e.g., zircon, baddeleyite) may provide insight into the geological provenance of minerals within sampled catchments.

The HMMA dataset comprises a staggering quantity of data and includes more than 140 million individual mineral grains observations across 1315 samples covering ~81 % of Australia. Given the scale of this multi-dimensional dataset, research into methods to facilitate rapid and effective exploration of HMMA data has progressed in parallel with data collection. Network analysis is a subfield of graph theory (Kolaczyk & Csárdi 2014) that has proven useful for visualising complex multidimensional systems and has been applied in the earth sciences in the form of mineral network analysis (MNA) (Morrison *et al.* 2017, Hazen *et al.* 2019, Morrison *et al.* 2020). Mineral data from the partial HMMA dataset releases has been integrated into a bespoke online Geoscience Australia-hosted MNA application (https://geoscienceaustralia.shinyapps.io/mna4hm/); the functionality of this application has been explained within Caritat *et al.* (2022) and will not be touched on further here. The application itself is a powerful tool that allows users to rapidly explore the HMMA dataset, and to discover relationships between minerals of interest with other minerals in sample assemblages as well as other forms of data (e.g. known mineral deposits).

[Approximate position of Fig. 11 here]

For Review Only

5. Conclusions

Production and analysis of the HMMA sample set required the development of an optimised sample processing workflow capable of producing 1315 samples within a non-commercial laboratory environment, the use of automated mineralogy, and the development of data visualisation tools. Sample processing, mounting and analysis took approximately 16 months. Workflow development considered a range of factors including time, sample reproducibility and minimisation of sample contamination. Innovative developments of the sample processing workflow included the use of 3-D printed sample georectification features, a 3-D printed riffle splitter, and a cryogenic process to accelerate heavy mineral separation. Classification of sample mineral content required automated mineralogy to deliver the substantial quantity of data required on a reasonable timescale and has produced a mineral library comprising more than 160 mineral phases across over 100 million unique mineral observations. Further, a mineral network analysis tool has been developed in parallel with data acquisition to facilitate exploration and knowledge discovery for a range of end users.

The Heavy Mineral Map of Australia project will be complete by October 2023. At its completion it will define a heavy mineral baseline across almost the entirety of Australia, and with it have generated an extensive heavy mineral sample archive that is hoped will be an important research resource for decades to come.

6. Acknowledgments

Geoscience Australia's Exploring for the Future program provides precompetitive information to inform decision-making by government, community and industry on the sustainable development of Australia's mineral, energy and groundwater resources. By gathering,

For Review Only

analysing and interpreting new and existing precompetitive geoscience data and knowledge, we are building a national picture of Australia's geology and resource potential. This leads to a strong economy, resilient society and sustainable environment for the benefit of all Australians. This includes supporting Australia's transition to net zero emissions, strong, sustainable resources and agriculture sectors, and economic opportunities and social benefits for Australia's regional and remote communities. The Exploring for the Future program, which commenced in 2016, is an eight year, $225m investment by the Australian Government. Patrice de Caritat and Evgeniy Bastrakov publish with permission from the Chief Executive Officer, Geoscience Australia.

The work was performed with the technical assistance of Anusha Shantha Kumara, Brad McDonald, Nasima Afrin Zinnia, Max Droellner and Payal Panchal. The Curtin TIMA instrument was funded by a grant from the Australian Research Council (LE140100150) and is managed by the John de Laeter Centre on behalf of a funding consortium including Curtin University, Geological Survey of Western Australia, University of Western Australia and Murdoch University.

For Review Only

7. References

Callahan J. (1987)

A nontoxic heavy liquid and inexpensive filters for separation of mineral grains. **Journal of Sedimentary Research**, 57(4).

Caritat P. de and Cooper M. (2011)

National Geochemical Survey of Australia: Data Quality Assessment. **Geoscience Australia Record 2011/021**. https://pid.geoscience.gov.au/dataset/ga/71971.

Caritat P. de and Cooper M. (2016)

A continental-scale geochemical atlas for resource exploration and environmental management: the National Geochemical Survey of Australia. **Geochemistry: Exploration, Environment, Analysis**, 16: 3-13. https://doi.org/10.1144/geochem2014-32.

Caritat P. de and Troitzsch U. (2021)

Towards a Regolith Mineralogy Map of the Australian Continent – A Feasibility Study in the Darling-Curnamona-Delamerian Region. **Geoscience Australia Record 2021/35**. http://dx.doi.org/10.11636/Record.2021.035.

Caritat P. de, Petts A. and Kelaart C. (2023)

Contribution Towards a Regolith Mineralogy Map of the Australian Continent A Study in South Australia, Queensland and the Northern Territory. **Geoscience Australia Record 2023/15**. https://dx.doi.org/10.26186/147990.

Caritat P. de, McInnes B.I., Walker A.T., Bastrakov E., Rowins S.M. and Prent A.M. (2022)

The Heavy Mineral Map of Australia: vision and pilot project. Minerals, 12(8), 961. https://doi.org/10.3390/min12080961.

Caritat P. de, Bastrakov E., Walker A.T. and McInnes B.I.A. (2022a)

The Heavy Mineral Map of Australia Project – Data Release 1: The Darling-Curnamona-Delamerian Region. **Geoscience Australia Record 2022/31**. http://dx.doi.org/10.11636/Record.2022.031 .

For Review Only

Caritat P. de, Bastrakov E., Walker A.T. and McInnes B.I.A. (2022b)

The Heavy Mineral Map of Australia Project – Data Release 2: The Barkly-Isa-Georgetown Region. **Geoscience Australia Record 2022/43**.

http://dx.doi.org/10.11636/Record.2022.043.

Cooper M., Caritat P. de., Burton G., Fidler R., Green G., House E., Strickland C., Tang J. and Wygralak A.S. (2010)

National Geochemical Survey of Australia: Field Data. **Geoscience Australia Record 2010/018**. https://pid.geoscience.gov.au/dataset/ga/70478.

Gurov E.P., Permiakov V. and Koeberl C. (2019)

Chromferide Found in Impact Melt Rocks of the El'gygytgyn Crater, Chukotka, Russia. In: **50th Annual Lunar and Planetary Science Conference**, 2132, p. 1347.

Hashmi S., Ward B.C., Plouffe A., Leybourne M.I. and Ferbey, T. (2015)

Geochemical and mineralogical dispersal in till from the Mount Polley Cu-Au porphyry deposit, central British Columbia, Canada. **Geochemistry: Exploration, Environment, Analysis**, 15(2-3), p. 234–249.

Hazen R.M., Downs, R.T., Eleish A., Fox P., Gagné O.C., Golden J.J., Grew E.S., Hummer D.R., Hystad G., Krivovichev S.V. and Li C. (2019)

Data-driven discovery in mineralogy: recent advances in data resources, analysis, and visualization. **Engineering**, 5(3), p. 397–405.

Hrstka T., Gottlieb P., Skala R., Breiter K. and Motl, D. (2018)

Automated mineralogy and petrology-applications of TESCAN Integrated Mineral Analyzer (TIMA). **Journal of Geosciences**, 63(1), 47–63.

For Review Only

Kolaczyk, E.D. and Csárdi, G. (2014)

Statistical analysis of network data with R (Vol. 65). **New York: Springer**.

Lau I., Bateman R., Beattie E., Caritat P. de, Thomas M., Ong C., Laukamp C., Caccetta M. Wang, R. and Cudahy T. (2016)

National Geochemical Survey of Australia reflectance spectroscopy measurements. v4. **CSIRO**. Data Collection. https://doi.org/10.25919/5cdba18939c29.

Lech M., Caritat P. de and McPherson A. (2007)

National Geochemical Survey of Australia: Field Manual. **Geoscience Australia Record 2007/008**. https://pid.geoscience.gov.au/dataset/ga/65234.

Lougheed H.D., McClenaghan M.B., Layton-Matthews D. and Leybourne M. (2020)

Exploration Potential of Fine-Fraction Heavy Mineral Concentrates from Till Using Automated Mineralogy: A Case Study from the Izok Lake Cu–Zn–Pb–Ag VMS Deposit, Nunavut, Canada. **Minerals**, 10(4), 310.

McClenaghan M.B. (2005)

Indicator mineral methods in mineral exploration. **Geochemistry: Exploration, Environment, Analysis**, 5(3), 233–245.

McClenaghan M.B. and Cabri L.J. (2011)

Review of gold and platinum group element (PGE) indicator minerals methods for surficial sediment sampling. **Geochemistry: Exploration, Environment, Analysis**, 11(4), 251–263.

Morrison S.M., Liu C., Eleish A., Prabhu A., Li C., Ralph J., Downs R.T., Golden J.J., Fox P., Hummer D.R. and Meyer M.B. (2017)

For Review Only

Network analysis of mineralogical systems. **American Mineralogist**, 102(8), pp.1588–1596.

Morrison S.M., Buongiorno J., Downs R.T., Eleish A., Fox P., Giovannelli D., Golden J.J., Hummer D.R., Hystad G., Kellogg L.H. and Kreylos O. (2020)

Exploring carbon mineral systems: recent advances in C mineral evolution, mineral ecology, and network analysis. **Frontiers in Earth Science**, p.208.

Morrow J.R. and Webster G.D (1989)

A cryogenic density separation technique for conodont and heavy mineral separations. **Journal of Paleontology**, 63(6), 953–955.

Novgorodova M.I., Gorshkov A.I., Trubkin N.V., Tsepin A.I. and Dimitrieva M.T. (1986)

New intermetallic compounds of iron and chromium-chromferide and ferchromide. Zap. Vses. **Mineral**. O-va, 115, 355–360.

Sexton M. (2011)

Australian Mineral Occurrences Collection. **Geoscience Australia Dataset**.

https://pid.geoscience.gov.au/dataset/ga/73131

Udayakumar S., Mohd Noor A.F., Sheikh Abdul Hamid S.A.R., Rama Putra T.A. and Anderson C.G. (2020)

Chemical and mineralogical characterization of Malaysian monazite concentrate. **Mining, Metallurgy & Exploration**, 37(2), 415–431.

Xie Y., Hou Z., Xu J., Yuan Z., Bai G. and Li X. (2006)

Discovery of Cu-Zn, Cu-Sn intermetallic minerals and its significance for genesis of the Mianning-Dechang REE metallogenic belt, Sichuan Province, China. **Science in China Series D**, 49(6), p. 597-603.

For Review Only

Data availability statement

The data related to the findings of this study will be publicly accessible from the Geoscience Australia web portal on the 12th October 2023.

Figure captions

Figure 1 – The HMMA sample preparation workflow.

Figure 2 – The 3-D printed riffle splitter used in the HMMA workflow.

Figure 3 – Finished sample mounts for the HMMA with embedded with three-sided reference frames on the upper surface and QR-coded sample labels on the back.

Figure 4 – Visualisations of the different TIMA scanning modes (after Hrstka *et al.* 2018).

Figure 5 – Excerpt from the HMMA TIMA mineral library. Mineral definitions utilise inclusionary, exclusionary, and ratio rules associated with the listed elements when classifying grain spectra.

Figure 6 – Sample panorama illustrating identified mineralogy across an analysed sample surface.

Figure 7 – BSE images of chromferide grains (highlighted in red) in two HMMA samples.

Figure 8 – BSE image of sub-ten-micron chromferide grain (highlighted in red, bottom left corner) in the control aliquot of silica sand.

For Review Only

Figure 9 – Presence (ticks) or absence (crosses) of selected minerals within original samples and paired site duplicates ('D').

Figure 10 – Scatter plots and least square regressions for Zr and zircon content (A), and Ti and equivalent rutile content (B).

Figure 11 – Distributions of cassiterite (SnO_2) occurrences within the HMMA BIG and DCD partial datasets, classified in eight quantile classes. Mineral deposit data: Sexton (2011).

Table captions

Table 1 – Differences (diff.) in mineral abundances between selected HMMA sites and their associated field duplicates (D). Abundances are expressed as individual mineral observations per sample with calculated percentage abundances per sample in brackets. 'Total' indicates total number of all mineral observations per sample.

Table 2 – Differences (diff.) in mineral abundances between selected HMMA samples and their manufactured duplicates. Abundances are expressed as individual mineral observations per sample with calculated percentage abundances per sample in brackets. 'Total' indicates total number of all mineral observations per sample.

Table 3 – Correlation coefficients between TOS (pilot) and BOS (HMMA) 75–*425* µm fractions after Box-Cox transformations for 12 selected minerals (bold: highest per row; red: highest per column; underlined: highest overall).

For Review Only

For Review Only

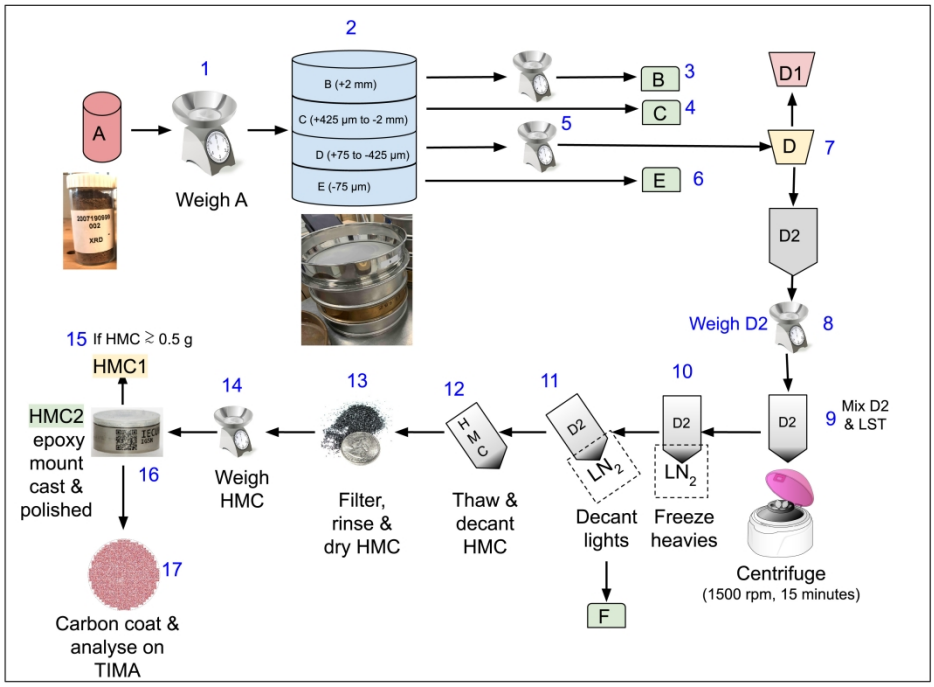

Figure 1 – The HMMA sample preparation workflow.

338x254mm (300 x 300 DPI)

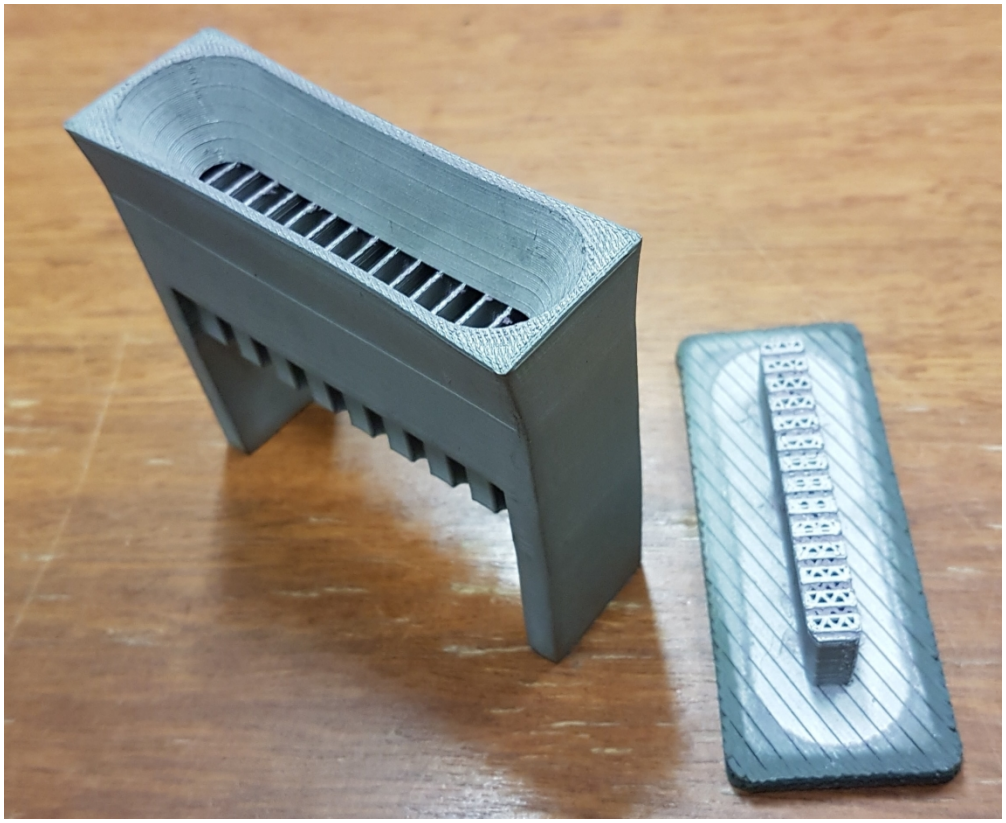

Figure 2 – The 3-D printed riffle splitter used in the HMMA workflow.

849x690mm (72 x 72 DPI)

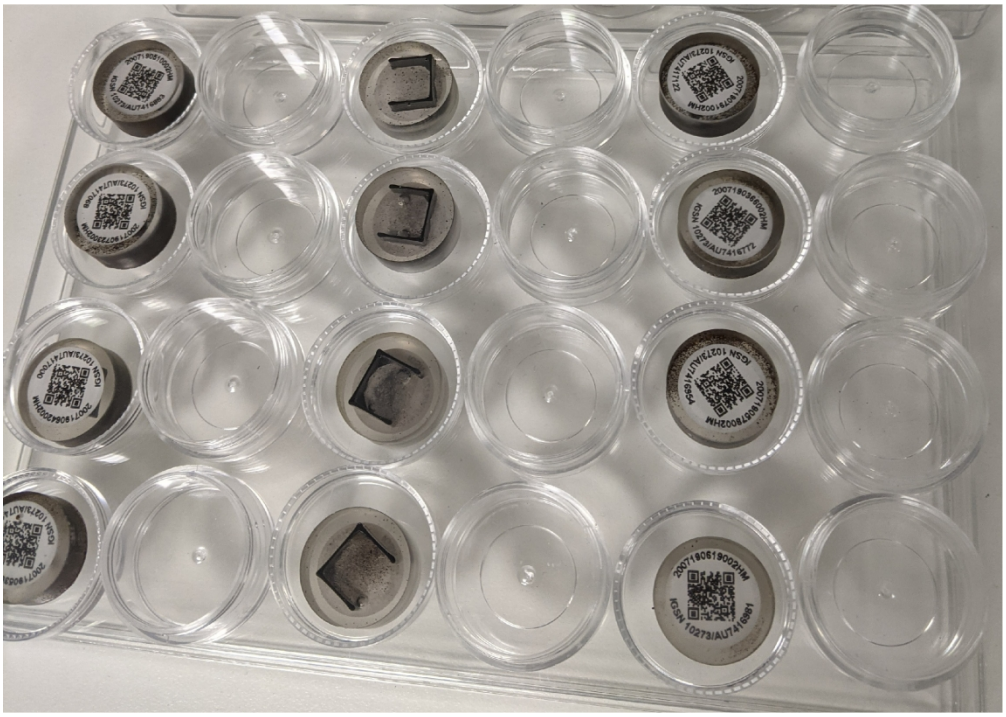

Figure 3 – Finished sample mounts for the HMMA with embedded with three-sided reference frames on the upper surface and QR-coded sample labels on the back.

198x140mm (300 x 300 DPI)

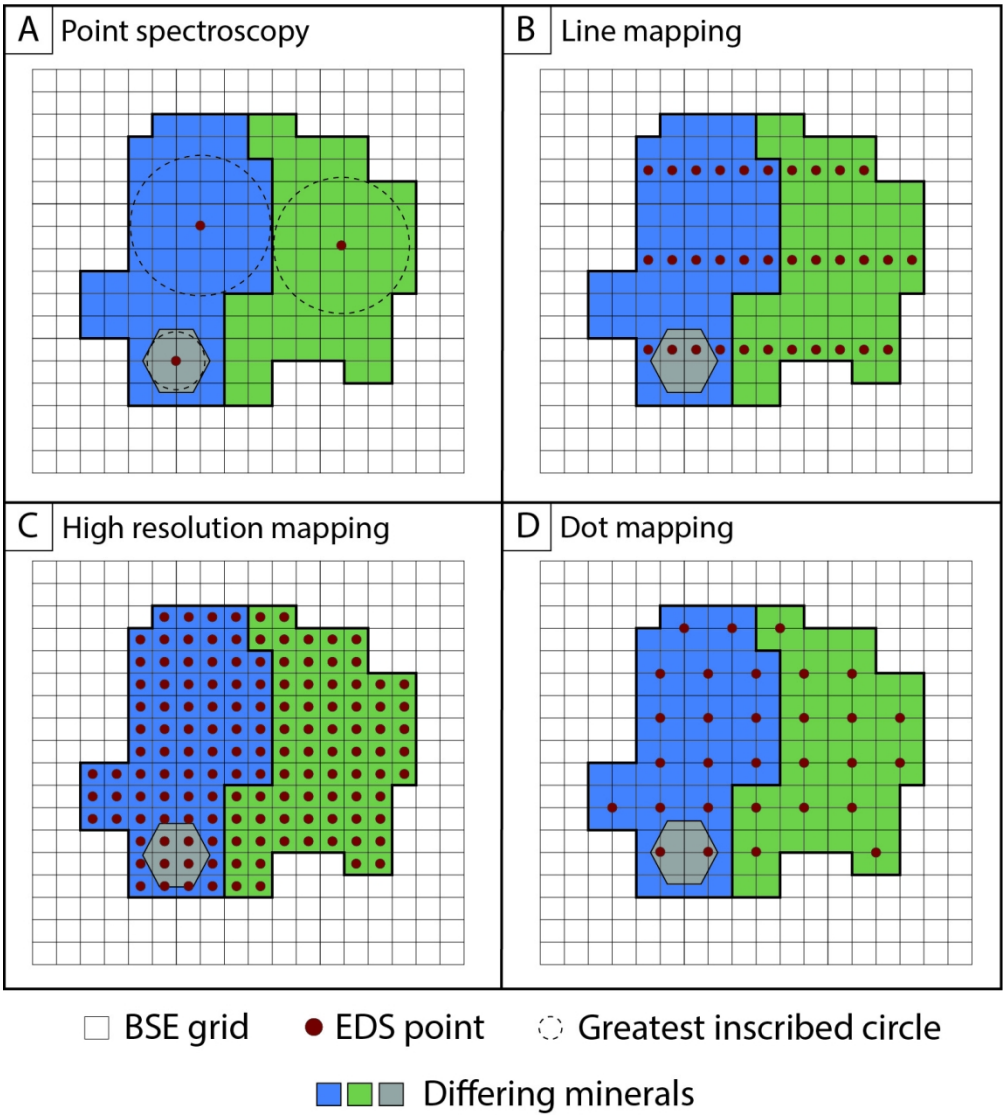

Figure 4 – Visualisations of the different TIMA scanning modes (after Hrstka et al. 2018).

134x149mm (300 x 300 DPI)

Name	Rules	Confidence [%]
Amphibole(Sadanagaite)	Na-K, Mg-K, Si-K, Al-K, Ca-K, Ti-K, K-K, O-K, Fe-K	99.50
Amphibole(Potassic-magnesiohastingsite)	Si-K, Ca-K, Mg-K, K-K, Na-K, Ti-K, Mn-K, Fe-K, O-K, Al-K	99.50
Amphibole(Katophorite)	Si-K, Na-K, Al-K, K-K, Ti-K, Mn-K, Fe-K, Mg-K, Ca-K, O-K	99.50
Ferrosaponite	Ca-K, Mg-K, Al-K, Si-K, O-K, Ti-K, Mn-K, K-K, Fe-K	99.50
Amphibole(Kaersutite)	Na-K, Ca-K, Mg-K, Ti-K, Si-K, Al-K, O-K, K-K, Fe-K	99.50
Arsenoflorencite	O-K, Al-K, P-K, S-K, La-L, As-K, Sr-K, Sr-L, Ce-L	99.50
Calcite	O-K, La-L, Ce-L, F-K, Ca-K, Sn-L, P-K, Mg-K, Si-K	99.99
Pumpellyite	O-K, Si-K, Ca-K, Al-K, Fe-K, K-K, Ti-K, La-L, Ce-L, Mn-K, Mg-K	99.50
Hematite/Magnetite	Al-K, Si-K, S-K, O-K, Cr-K, Fe-K / O-K, Fe-K, Mg-K, Mn-K, Ti-K	99.99
Piemontite	Mn-K, Ti-K, Al-K, Si-K, O-K, Ca-K, K-K, Mg-K, Fe-K	99.50
Pyroxene(Augite)	O-K, Al-K, Mg-K, Na-K, K-K, Ca-K, Ti-K, Si-K, Fe-K	99.50
Pyroxene(Diopside-Hedenbergite)	Si-K, O-K, Ca-K, Na-K, K-K, Al-K, W-L, Mg-K + Fe-K	99.50
Garnet(Almandine)	O-K, Si-K, Al-K, Fe-K, Ca-K, Mg-K, Mn-K, K-K, Si-K / Al-K, S-K, P-K, W-L	98.00
Plumbogummite	Al-K, P-K, O-K, Pb-M	99.50
Hollandite	Mn-K, Ba-L, Na-K, Fe-K, Pb-L, O-K, Al-K, Si-K	99.50
Pyroxene(Jadeite)	O-K, Si-K, Al-K, Na-K, Ca-K, Ti-K, K-K, Fe-K	99.50
Amphibole(Ferropargasite)	Mg-K, Na-K, Ca-K, Al-K, Si-K, O-K, K-K, Fe-K	99.50
Amphibole(Taramite)	O-K, Al-K, Si-K, Na-K, Mg-K, K-K, Ca-K, Mn-K, Ti-K, Fe-K	99.50
Amphibole(Fluoropargasite)	Na-K, Ca-K, Al-K, Si-K, O-K, K-K, Fe-K, Mg-K	99.50

Figure 5 – Excerpt from the HMMA TIMA mineral library. Mineral definitions utilise inclusionary, exclusionary, and ratio rules associated with the listed elements when classifying grain spectra.

195x121mm (96 x 96 DPI)

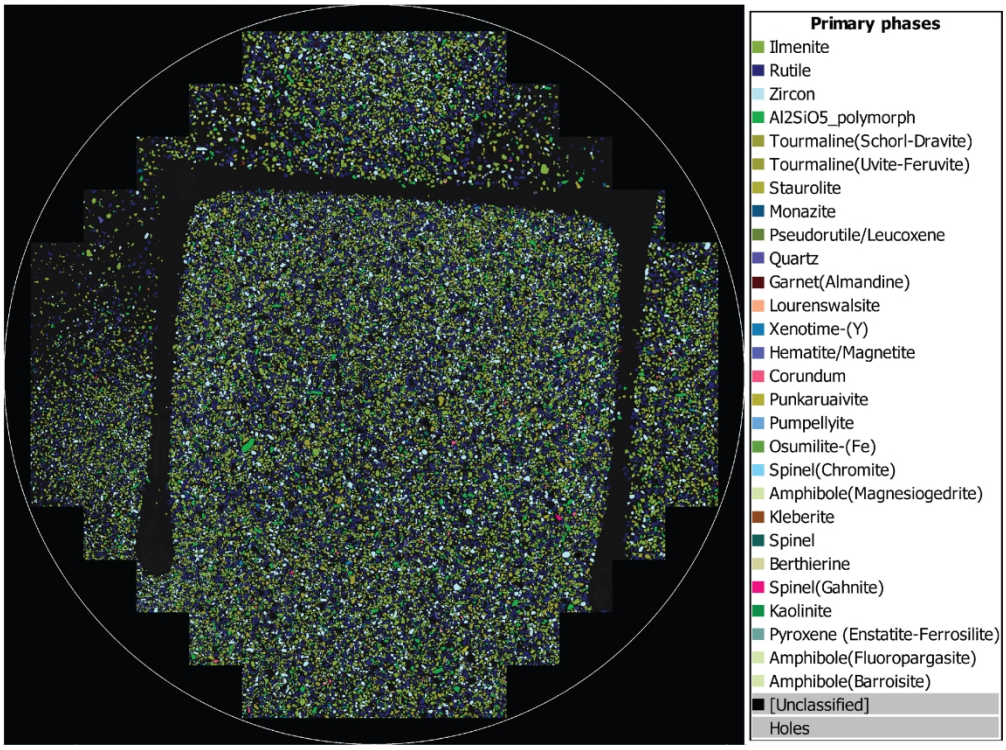

Figure 6 – Sample panorama illustrating identified mineralogy across an analysed sample surface.

260x193mm (300 x 300 DPI)

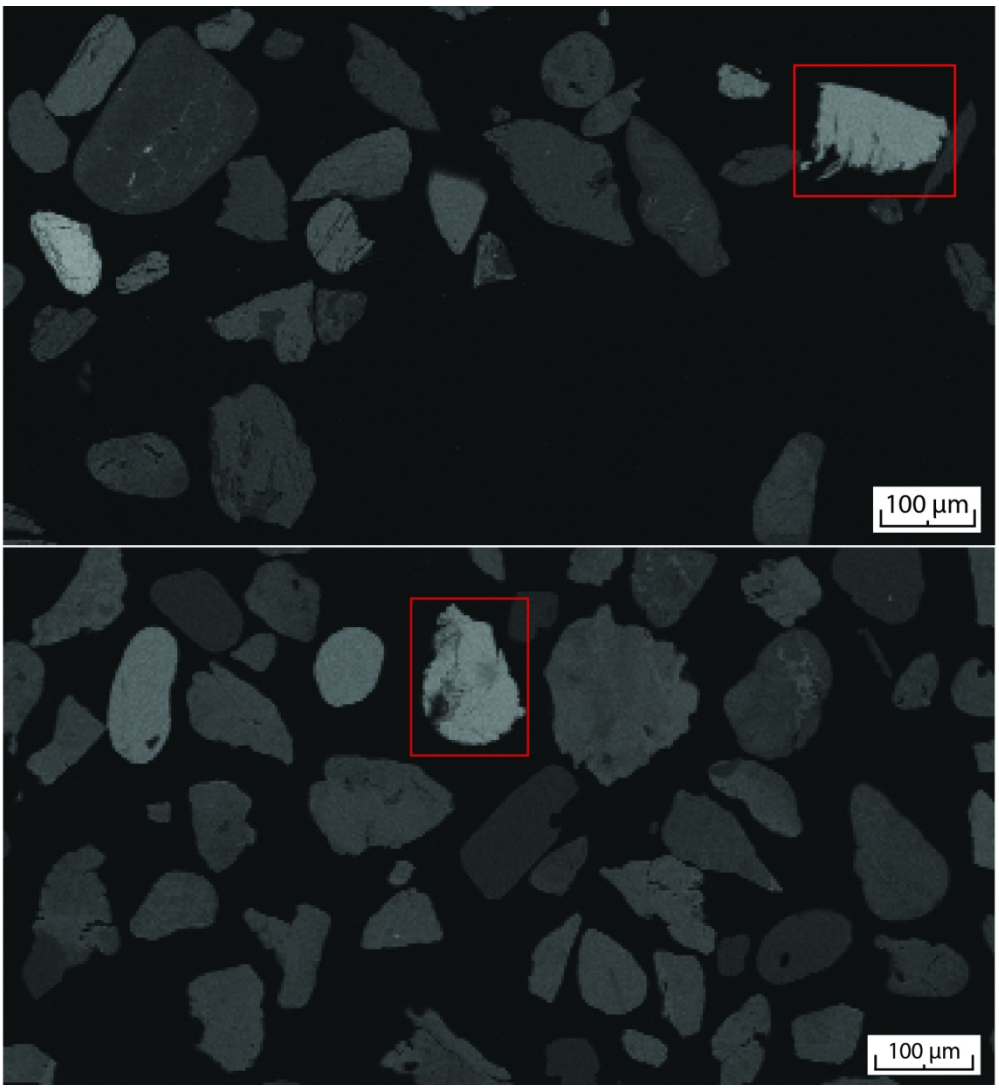

Figure 7 – BSE images of chromferide grains (highlighted in red) in two HMMA samples.

157x169mm (300 x 300 DPI)

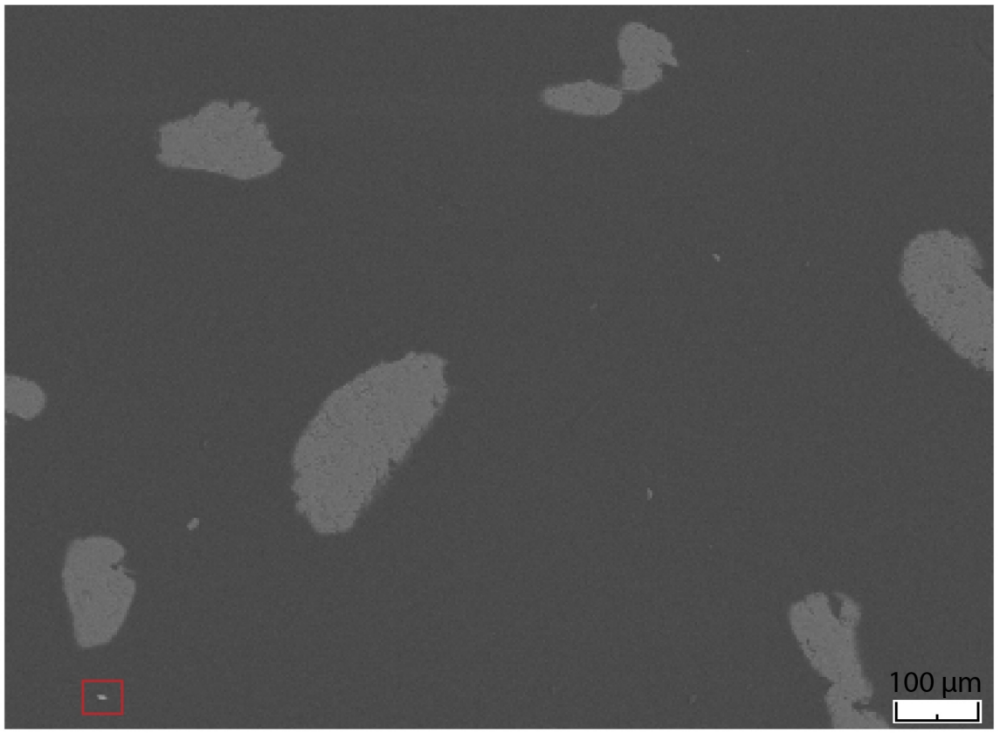

Figure 8 – BSE image of sub-ten-micron chromferide grain (highlighted in red, bottom left corner) in the control aliquot of silica sand.

140x102mm (300 x 300 DPI)

Sample	Chromite	Florencite	Gahnite	Ilmenite	Rutile	Zircon
2007190003	✗	✓	✗	✓	✓	✓
2007190213(D)	✓	✓	✓	✓	✓	✓
2007190005	✓	✓	✓	✓	✓	✓
2007191059(D)	✓	✓	✗	✓	✓	✓
2007190032	✓	✓	✓	✓	✓	✓
2007190632(D)	✓	✓	✓	✓	✓	✓
2007190035	✓	✓	✓	✓	✓	✓
2007190876(D)	✓	✓	✓	✓	✓	✓
2007190039	✓	✓	✗	✓	✓	✓
2007190984(D)	✓	✓	✗	✓	✓	✓
2007190050	✓	✓	✓	✓	✓	✓
2007191481(D)	✓	✓	✓	✓	✓	✓

Figure 9 – Presence (ticks) or absence (crosses) of selected minerals within original samples and paired site duplicates ('D').

147x126mm (300 x 300 DPI)

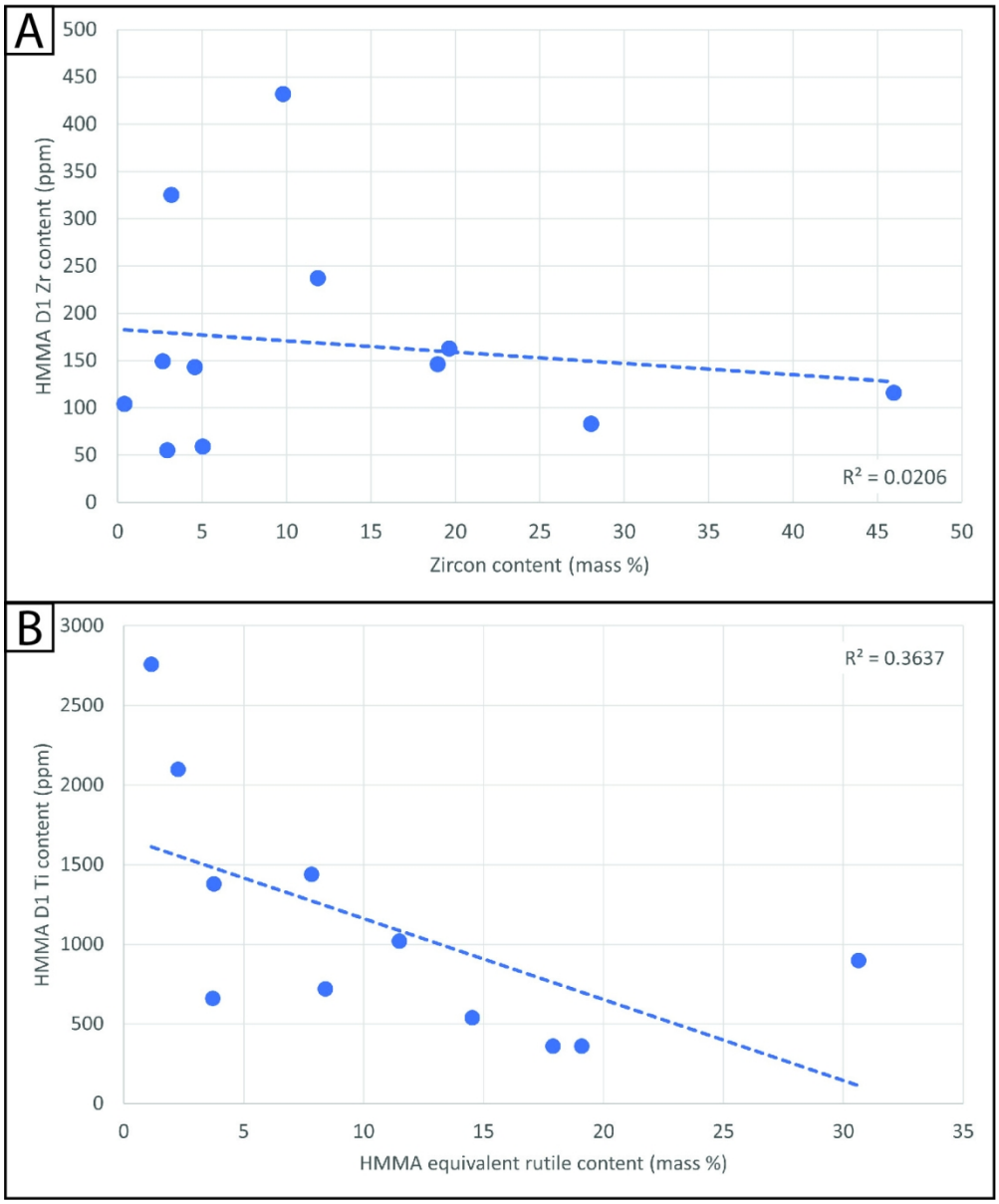

Figure 10 – Scatter plots and least square regressions for Zr and zircon content (A), and Ti and equivalent rutile content (B).

136x163mm (300 x 300 DPI)

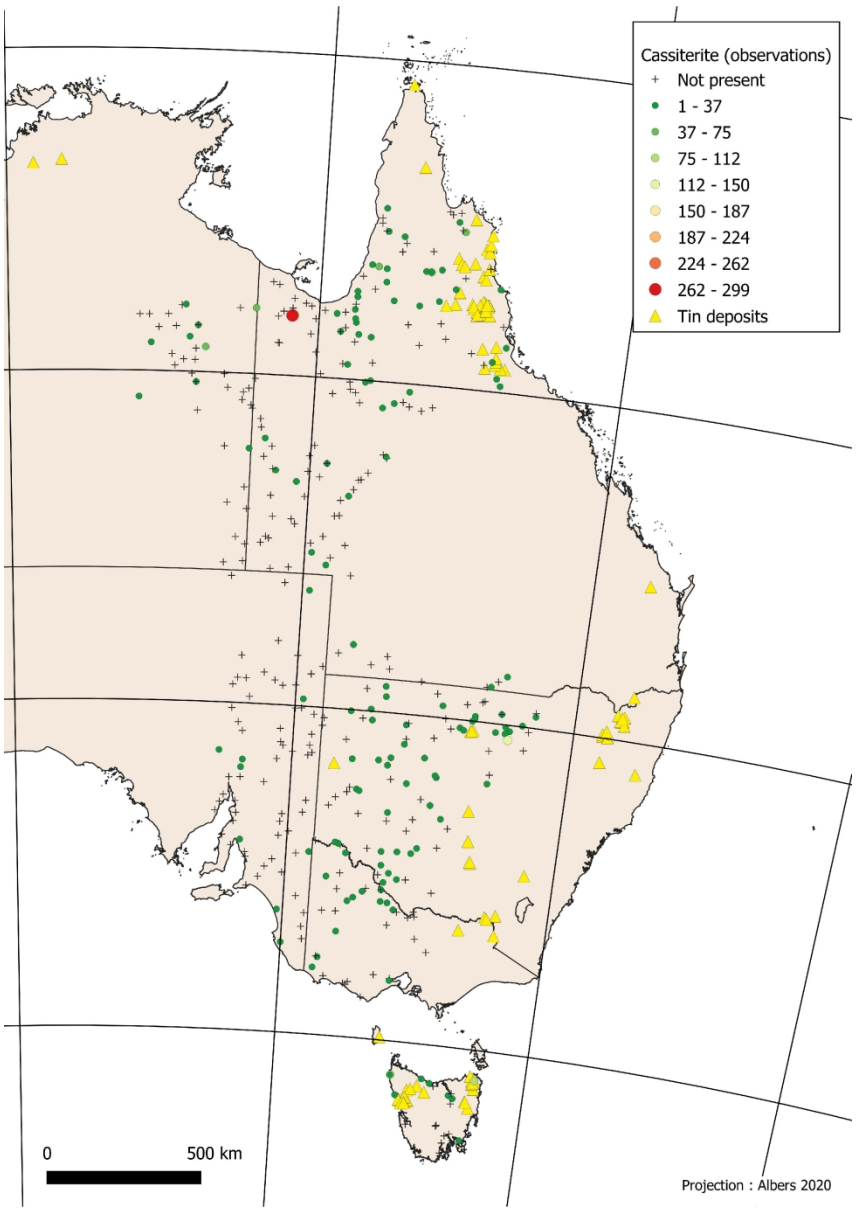

Figure 11 – Distributions of cassiterite (SnO_2) occurrences within the HMMA BIG and DCD partial datasets, classified in eight quantile classes. Mineral deposit data: Sexton (2011).

209x297mm (300 x 300 DPI)

Sample	Chromite	Florencite	Gahnite	Ilmenite
2007190003	0 (0%)	1 (0%)	0 (0%)	1472 (2.5%)
2007190213(D)	21 (0%)	9 (0%)	1 (0%)	8462 (4.8%)
diff.	0%	0%	0%	2.30%
2007190005	238 (0.2%)	262 (0.2%)	14 (0%)	11523 (9.4%)
2007191059(D)	335 (0.1%)	232 (0.1%)	0 (0%)	28216 (12.4%)
diff.	-0.10%	-0.10%	0%	3%
2007190032	273 (0.2%)	61 (0%)	1 (0%)	34305 (22.1%)
2007190632(D)	148 (0.1%)	41 (0%)	1 (0%)	29562 (19.1%)
diff.	-0.10%	0%	0%	-3%
2007190035	143 (0.1%)	22 (0%)	8 (0%)	16669 (9.1%)
2007190876(D)	68 (0%)	23 (0%)	1 (0%)	12453 (7%)
diff.	-0.10%	0%	0%	-2.10%
2007190039	13 (0%)	9 (0%)	0 (0%)	1845 (3.9%)
2007190984(D)	19 (0%)	5 (0%)	0 (0%)	3384 (6.9%)
diff.	0%	0%	0%	-3%
2007190050	564 (0.5%)	7 (0%)	4 (0%)	6942 (5.9%)
2007191481(D)	451 (0.3%)	3 (0%)	6 (0%)	5796 (3.5%)
diff.	-0.20%	0%	0%	-2.40%

For Review Only

Rutile	Zircon	Total
593 (1%)	99 (0.2%)	59595
2873 (1.6%)	1033 (0.6%)	175993
0.60%	0.40%	
6159 (5%)	895 (0.7%)	122703
6573 (2.9%)	1099 (0.5%)	227577
-2.10%	-0.20%	
15535 (10%)	3235 (2.1%)	155291
12393 (8%)	2109 (1.4%)	155074
-2%	-0.70%	
8445 (4.6%)	2860 (1.6%)	182279
7098 (4%)	2158 (1.2%)	176757
-0.60%	-0.40%	
1095 (2.3%)	723 (1.5%)	47663
1552 (3.2%)	1629 (3.3%)	49012
0.90%	1.80%	
5838 (4.9%)	2346 (2%)	118141
6212 (3.7%)	1309 (0.8%)	167420
-1.20%	-1.20%	

For Review Only

Sample	Chromite	Florencite	Gahnite	Ilmenite
2007191434	3 (0%)	0 (0%)	1 (0%)	1174 (0.7%)
Lab Duplicate	2 (0%)	0 (0%)	0 (0%)	2139 (1.2%)
diff.	0%	0%	0%	0.50%
2007191503	1 (0%)	15 (0%)	1 (0%)	1968 (1.6%)
Lab Duplicate	3 (0%)	7 (0%)	0 (0%)	1215 (1.7%)
diff.	0%	0%	0%	0.10%
2007191262	11 (0%)	41 (0%)	15 (0%)	15952 (12%)
Lab Duplicate	11 (0%)	25 (0%)	11 (0%)	16059 (15.5%)
diff.	0%	0%	0%	3.50%
2007191286	8 (0%)	2 (0%)	0 (0%)	2655 (2.4%)
Lab Duplicate	11 (0%)	2 (0%)	1 (0%)	1749 (1.3%)
diff.	0%	0%	0%	-1.10%
2007191310	0 (0%)	40 (0%)	0 (0%)	7541 (3.1%)
Lab Duplicate	1 (0%)	33 (0%)	0 (0%)	5634 (3.8%)
diff.	0%	0%	0%	0.70%
2007191372	4 (0%)	10 (0%)	3 (0%)	18193 (21%)
Lab Duplicate	20 (0%)	13 (0%)	1 (0%)	29989 (32.5%)
diff.	0%	0%	0%	11.50%

For Review Only

Rutile	Zircon	Total
422 (0.3%)	94 (0.1%)	160874
544 (0.3%)	184 (0.1%)	174972
0%	0%	
2603 (2.1%)	323 (0.3%)	126565
1110 (1.5%)	250 (0.3%)	72176
-0.50%	0%	
2229 (1.7%)	1568 (1.2%)	133409
1290 (1.2%)	1651 (1.6%)	103804
-0.50%	0.40%	
1311 (1.2%)	444 (0.4%)	109544
755 (0.6%)	265 (0.2%)	133930
-0.60%	-0.20%	
5609 (2.3%)	547 (0.2%)	239982
3844 (2.6%)	936 (0.6%)	149620
0.30%	0.40%	
6059 (7%)	1241 (1.4%)	86483
6003 (6.5%)	2598 (2.8%)	92153
-0.50%	1.40%	

For Review Only

Mineral	Observations	Volume percent	Weight percent
Almandine	**0.9**	0.85	0.85
Biotite	0.91	0.93	**0.96**
Corundum	**0.83**	0.81	0.76
Hematite/Magnetite	0.81	0.84	**0.86**
Ilmenite	0.27	0.75	**0.78**
Monazite	0.46	**0.85**	0.84
Punkaruaivite	0.78	**0.91**	**0.91**
Rutile	0.6	**0.9**	**0.9**
Schorl-Dravite	0.19	0.92	**0.94**
Staurolite	0.77	0.91	**0.96**
Xenotime-Y	0.39	0.71	**0.74**
Zircon	0.29	**0.54**	0.47

For Review Only